Platelet secretion and hemostasis require syntaxin-binding protein STXBP5

Shaojing Ye,[1] Yunjie Huang,[1] Smita Joshi,[1] Jinchao Zhang,[1] Fanmuyi Yang,[2] Guoying Zhang,[2] Susan S. Smyth,[2] Zhenyu Li,[2] Yoshimi Takai,[3] and Sidney W. Whiteheart[1]

[1]Department of Molecular and Cellular Biochemistry and [2]Department of Internal Medicine, University of Kentucky College of Medicine, Lexington, Kentucky, USA. [3]Department of Biochemistry and Molecular Biology, Kobe University Graduate School of Medicine, Kobe, Japan.

Genome-wide association studies (GWAS) have linked genes encoding several soluble NSF attachment protein receptor (SNARE) regulators to cardiovascular disease risk factors. Because these regulatory proteins may directly affect platelet secretion, we used SNARE-containing complexes to affinity purify potential regulators from human platelet extracts. Syntaxin-binding protein 5 (STXBP5; also known as tomosyn-1) was identified by mass spectrometry, and its expression in isolated platelets was confirmed by RT-PCR analysis. Coimmunoprecipitation studies showed that STXBP5 interacts with core secretion machinery complexes, such as syntaxin-11/SNAP23 heterodimers, and fractionation studies suggested that STXBP5 also interacts with the platelet cytoskeleton. Platelets from *Stxbp5* KO mice had normal expression of other key secretory components; however, stimulation-dependent secretion from each of the 3 granule types was markedly defective. Secretion defects in STXBP5-deficient platelets were confirmed via lumi-aggregometry and FACS analysis for P-selectin and LAMP-1 exposure. Interestingly, STXBP5-deficient platelets had altered granule cargo levels, despite having normal morphology and granule numbers. Consistent with secretion and cargo deficiencies, *Stxbp5* KO mice showed dramatic bleeding in the tail transection model and defective hemostasis in the $FeCl_3$-induced carotid injury model. Transplantation experiments indicated that these defects were due to loss of STXBP5 in BM-derived cells. Our data demonstrate that STXBP5 is required for normal arterial hemostasis, due to its contributions to platelet granule cargo packaging and secretion.

Introduction

Cardiovascular diseases, such as myocardial infarction, stroke, and deep vein thrombosis, are leading causes of death and disability. These potentially occlusive processes are influenced in part by platelet secretion (1, 2). As a physiological response to vascular damage, platelets are activated and secrete components that promote thrombus formation and initiate its sequelae, e.g., wound healing and angiogenesis (1, 3, 4). Platelet secretion is mediated by highly conserved soluble *N*-ethylmaleimide–sensitive factor (NSF) attachment protein receptor (SNARE) proteins: vesicle/granule SNAREs (v-SNAREs) consist of the vesicle-associated membrane proteins (VAMPs), and target membrane SNAREs (t-SNAREs) consist of 2 classes, syntaxins and members of the synaptosomal-associated protein 23/25 (SNAP23/25) family. A *trans*-membrane complex of these 3 proteins mediates bilayer fusion and thus granule cargo release (5). In human and mouse platelets, this core fusion complex includes VAMP8, SNAP23, and syntaxin-11 (STX11) (6–9). These core elements are acted on by regulatory proteins, which affect when and where SNARE interactions occur. This assures physiologically relevant secretion (10, 11). In platelets, syntaxin regulators such as Munc18b and tethering proteins such as Munc13-4 and Rab27 are required for granule release (1, 12, 13). Genome-wide association studies (GWAS) have linked other secretory regulators to cardiovascular diseases (14–20); thus, to understand the significance of these associations, it is important to determine which types of SNARE regulators control platelet secretion.

In our continuing effort to identify new secretion regulators, we used t-SNARE–containing complexes to capture SNARE-binding proteins from platelet extracts. We identified syntaxin-binding protein 5 (STXBP5; also known as tomosyn-1 [i.e., "friend of syntaxin"]) as a novel candidate for affecting platelet secretion. STXBP5 is a 130-kDa protein that was originally identified as a STX1-binding partner in neuronal tissue (21). Subsequent studies have shown that STXBP5 interacts with other syntaxin isoforms and is widely expressed (22). STXBP5 belongs to a family of WD40 repeat–containing proteins associated with exocytosis and with the actin cytoskeleton: Sro7/Sro77 in yeast, Tom1 in *C. elegans*, and STXBP5 in mammals (23–28). In mammals, 2 genes are present, *Stxbp5* and *Stxbp5l* (also known as *Tomosyn-2*), and alternative splicing produces 7 protein isoforms (29, 30). STXBP5 has 3 isoforms, based on molecular weight: big, middle, and small (b-STXBP5, m-STXBP5, and s-STXBP5, respectively). Structurally, STXBP5 is composed of an N-terminal WD40 repeat (~90% of the total protein sequence), a highly variable linker region, and a C-terminal v-SNARE (or R-SNARE) motif (30). The v-SNARE motif is proposed to exert a negative effect on fusogenic SNARE complex assembly by blocking v-SNARE binding to t-SNAREs (31). Consistently, overexpression of STXBP5 in neurons and neuroendocrine secretory cells inhibits exocytosis, and gene mutations in *C. elegans* or genetic deple-

▶ Related Commentary: p. 4231

Conflict of interest: Yoshimi Takai serves on scientific advisory boards for, and has received consulting fees from, Kan Research Institute Inc. and Asubio Pharma Co.
Submitted: February 5, 2014; **Accepted:** July 24, 2014.
Reference information: *J Clin Invest*. 2014;124(10):4517–4528. doi:10.1172/JCI75572.

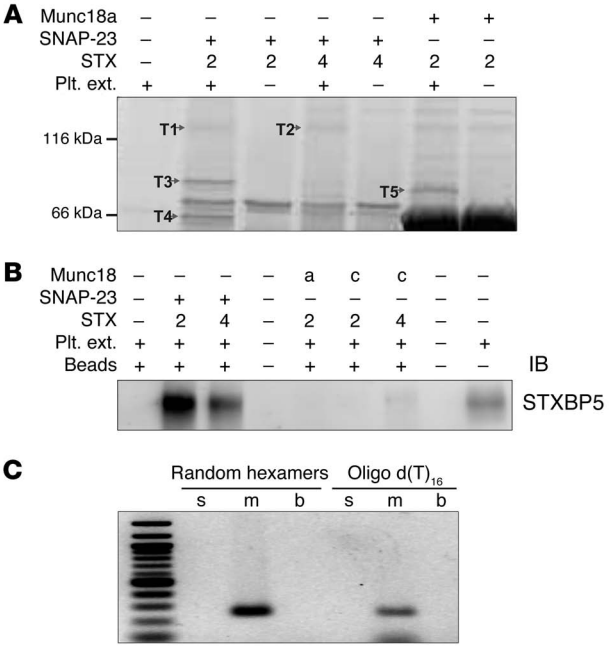

Figure 1. STXBP5 is present in human platelets. (**A**) The indicated complexes were produced in *E. coli* using the pRSFDuet plasmid with the S-tag peptide fused to the C terminus of the syntaxin. Complexes were bound to protein S agarose beads. After washing, the complex-bound beads were incubated with solubilized human platelet extracts (Plt. ext.). The beads were washed again, and the proteins were eluted with SDS-PAGE loading buffer. The eluted proteins were separated by SDS-PAGE and stained with Sypro Ruby. The specific interacting proteins (T1–T5) were excised, subjected to trypsin digestion, and analyzed by mass spectrometry. The spectra were searched using MASCOT software (see Supplemental Table 1 for search results). (**B**) The indicated complexes were produced in *E. coli* using the pRSFDuet plasmid with the S-tag peptide fused to the C terminus of the syntaxin. Solubilized human platelet extracts were incubated with the different complexes, and the resulting material was recovered on protein S agarose beads. After washing, the proteins were eluted and probed with anti-STXBP5 mAb. (**C**) Analysis of STXBP5 isoforms by RT-PCR. The human platelet–derived mRNA was converted to cDNA and preamplified by using either random hexamers or oligo $d(T)_{16}$ primers, followed by regular PCR using isoform-specific primers for s-STXBP5, m-STXBP5, and b-STXBP5 (see Methods). The 1-kb DNA ladder standard is at the far left.

tion of *Stxbp5* in mice enhances synaptic transmission (24, 32, 33). However, the N-terminal domain of STXBP5, lacking the syntaxin-binding v-SNARE motif, can also inhibit secretion from PC-12 cells, which suggests that other interactions with STXBP5 are important (33). Conversely, knockdown of STXBP5 in superior cervical ganglion neurons (34) and in the rat β cell line INS-1E (35), and genetic depletion of the homologs Sro7 and Sro77 in yeast (25), negatively affects exocytosis. Thus, although STXBP5 may be a negative regulator of secretion in some cells, it may play a positive role in others (24). To date, the role of this potential SNARE regulator in platelets has not been addressed.

Various studies have linked STXBP5 with neuropsychological and cardiovascular diseases in humans. Deletions in the *Stxbp5* gene are linked to autism (36). GWAS show genetic variations in *Stxbp5* are linked with increased plasma levels of vWF (14–19), alterations in tissue plasminogen activator (tPA) levels (20), venous thrombosis (16), and arterial thrombosis (19). Specifically, 1 SNP that produces a nonsynonymous mutation (N436S) was associated with increased bleeding (18). These associations suggest a role for STXBP5 in both endothelial cell (EC) and platelet secretion and point to a role for the protein in normal hemostasis. In the present study, we examined the platelet phenotype of mice lacking STXBP5 to understand how this t-SNARE regulator affects platelet exocytosis, granule biogenesis, and hemostasis.

Results

STXBP5 is present in human platelets. The critical SNAREs in platelets have been identified: STX11 and SNAP23 as the t-SNAREs, and VAMP8 as the primary v-SNARE (6, 8, 9). Of these 3 SNARE types, syntaxins and their binding proteins have dominated the ranks of potential secretion regulators, which suggests that syntaxins or syntaxin-containing complexes might serve as useful "bait" to identify additional secretion regulators. Because of our problems with the insolubility of STX11 when expressed in bacteria (S. Ye and J. Zhang, unpublished observation), STX2 and STX4 were used as surrogates to create syntaxin-SNAP23 and syntaxin-Munc18 complexes for pulldown assays. Using human platelet extracts and various syntaxin-containing complexes as bait, we recovered 5 bands that represented proteins specifically bound to 1 or more of the syntaxin-containing baits used (Figure 1A). Mass spectrometry analysis showed that bands T1 and T2 were STXBP5, band T3 was phosphofructokinase C, band T4 was Munc18b, and band T5 was granuphilin (also known as SLP4) (Figure 1 and Supplemental Table 1; supplemental material available online with this article; doi:10.1172/JCI75572DS1). Munc18b is known to be required for platelet secretion and to bind to t-SNARE complexes (13, 37). Granuphilin is a known Rab27 effector and is important for dense granule secretion (12, 38). The role of phosphofructokinase is unclear at present. STXBP5 has been shown to be involved in neuronal and neuroendocrine exocytosis (21, 24, 39). Platelet STXBP5 (bands T1 and T2) was specifically associated with t-SNARE heterodimers, consistent with previous reports showing that STXBP5 forms ternary complexes with STX4/SNAP23 and STX1/SNAP25 (22, 31). To verify STXBP5 expression in human platelets and our mass spectrometry results, we probed platelet extracts and affinity-purified complexes by IB using an anti-STXBP5 peptide mAb (whose epitope is a region shared by all 3 isoforms). A specific immunoreactive band was only seen in samples bound to the t-SNARE heterodimers, not in those bound to Munc18a- or Munc18c-containing complexes (Figure 1B). To determine which STXBP5 isoforms were present in human platelets, RT-PCR analysis was performed using random hexamers and oligo d(T) to prime the reverse transcription step, then using isoform-specific primers for PCR (29, 40). Only primers for m-STXBP5 produced a product (Figure 1C), which suggests that m-STXBP5 is the most abundant isoform in platelets. Expression of STXBP5 has been consistently reported previously, in the mass spectrometry analysis of the human platelet proteome by Burkhart et al. (41) and in a genome-wide RNA sequence analysis of human and mouse platelets by Rowley et al. (42).

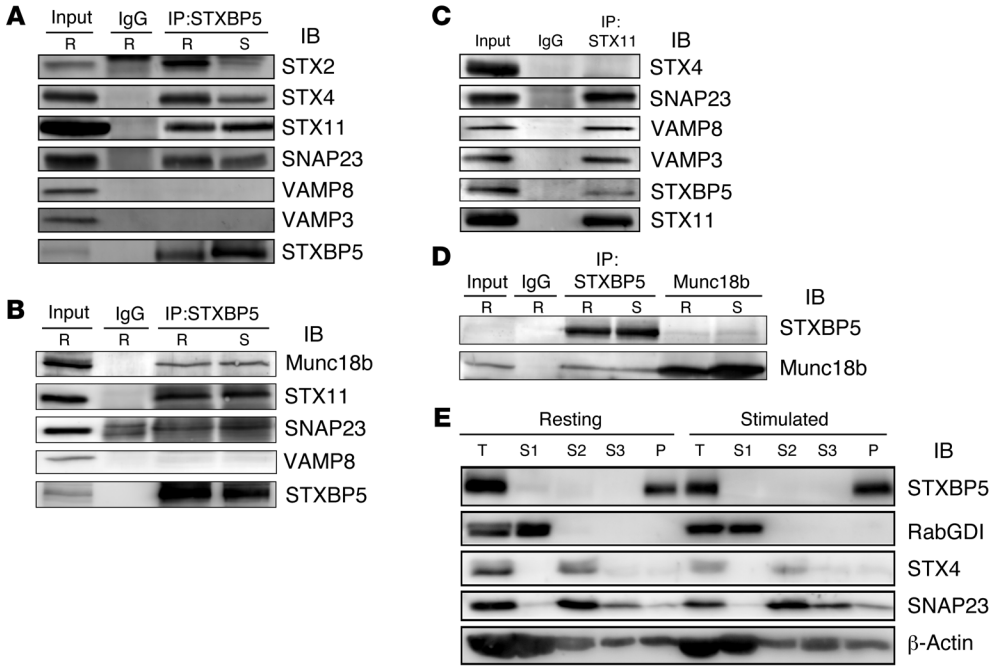

Figure 2. STXBP5 is associated with platelet SNARE complexes and cytoskeleton. (**A**–**D**) Platelet extracts (Input) from resting (R) or thrombin-stimulated (S) platelets were prepared by solubilization with 1% Triton X-100. After clarification, platelet extracts were incubated with anti-STXBP5 mAb (**A**) or rabbit polyclonal Ab (**B** and **D**), anti-STX11 rabbit polyclonal Ab (**C**), anti-Munc18b goat polyclonal Ab (**D**), or IgG control for 3 hours at 4°C. Immune complexes were recovered with protein A and G sepharose. The bound proteins were eluted and separated by SDS-PAGE, followed by IB with the indicated antibodies. (**E**) Washed platelets (2.5×10^8) were resuspended in HEPES/Tyrode buffer and incubated with (stimulated) or without (resting) 0.1 U/ml thrombin for 5 minutes. After disruption by freeze-thaw, the unbroken cells were removed by centrifugation at 700 *g* for 5 minutes, and supernatants were subjected to ultracentrifugation (100,000 *g* for 1 hour at 4°C). The cytosolic fractions (S1) were collected. The remaining pellets were solubilized sequentially with Triton X-100 (S2), then *n*-octyl-β-D-glucopyranoside (S3). The supernatants and insoluble pellet (P) were analyzed by IB with the indicated antibodies. T, total extract (starting material for the fractionation).

STXBP5 is associated with platelet SNARE machinery. To demonstrate that STXBP5 does interact with the functionally relevant syntaxin isoform in platelets, STX11 (as well as SNAP23 and VAMP8), we immunoprecipitated endogenous STXBP5 from detergent-solubilized extracts and probed the precipitate with antibodies against known elements of the platelet secretory machinery. Both resting and thrombin-stimulated human platelets were lysed with Triton X-100, and immunoprecipitation was performed using nonspecific IgG or an anti-STXBP5 mAb. It should be noted that much of the platelets STXBP5 was in the pellet fraction under these conditions; however, we chose to focus only on the soluble pool, so as to lessen the chance of detecting artifactual interactions due to incomplete solubilization. IB showed that the t-SNAREs STX11 and SNAP23 were recovered in the STXBP5 immunoprecipitates (Figure 2, A and B). Reciprocal immunoprecipitation with anti-STX11 antibodies confirmed this interaction (Figure 2C). In agreement with the in vitro pulldown results (Figure 1A), endogenous STXBP5 could also bind STX2 and STX4. No VAMP3 or VAMP8 was detected, consistent with the notion that STXBP5 competes with v-SNAREs to bind t-SNARE complexes (31). Another platelet secretory component, Munc18b, was coimmunoprecipitated with STXBP5 (Figure 2B). Reciprocal immunoprecipitation confirmed the STXBP5/Munc18b interaction (Figure 2D). At this stage, it was not mechanistically clear why the complex composition was unaffected by platelet activation. Regardless, these data showed that STXBP5 associated with the critical secretory components SNAP23, STX11, and Munc18b in platelets and that its association was exclusive of the VAMPs.

STXBP5 localization in platelets. We next sought to determine the distribution of STXBP5 in platelets using biochemical fractionation and immunofluorescence microscopy. Resting and thrombin-activated platelets were disrupted by repeated freeze-thaw and separated into cytosolic and pelleted fractions by centrifugation (Figure 2E). The pelleted fractions were extracted sequentially with Triton X-100 and *n*-octyl-β-D-glucopyranoside to solubilize membrane proteins and lipid raft components, respectively. The cytosolic marker RabGDI fractionated into the first supernatant, and the membrane protein marker STX4 was found in the Triton X-100–solubilized fraction. The raft marker SNAP23 was present both in the Triton X-100–solubilized fraction and in the *n*-octyl-β-D-glucopyranoside–solubilized fraction. STXBP5 was found in the final cytoskeletal pellet, consistent with actin's presence (43). The distribution of STXBP5 in platelets (spread on fibrinogen-coated coverslips) was also suggestive of interaction with the cytoskeleton. STXBP5 was concentrated in the central region of the platelets and was surrounded by phalloidin-stained actin filaments (Figure 3, A–D). Because these platelets were surface-activated by spreading on coated glass, few granules remained, but P-selectin staining did appear in the central area of some platelets (Figure 3, A–D), consistent

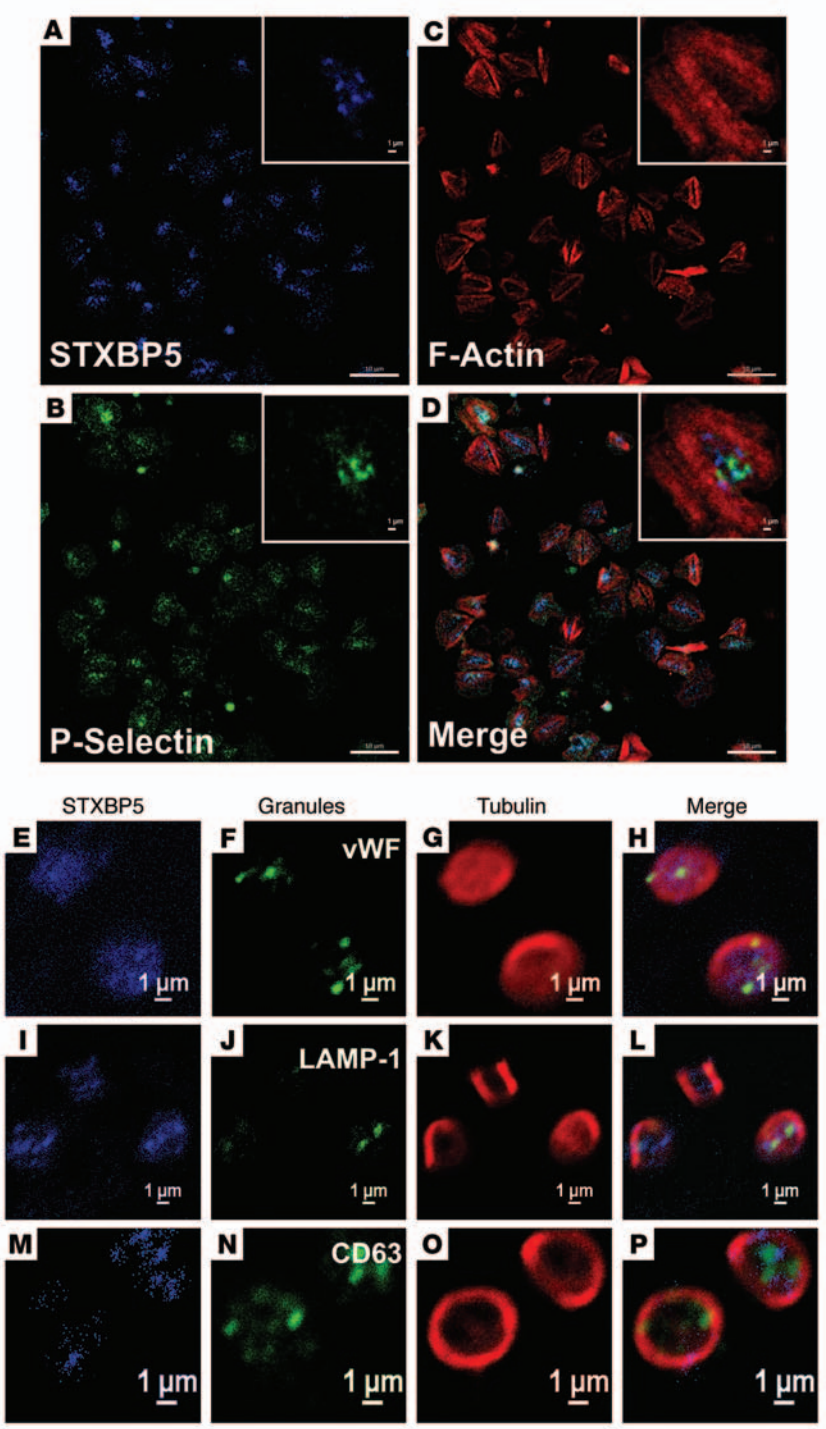

Figure 3. STXBP5 is present in platelets. Washed human platelets were allowed to bind to fibrinogen-coated coverslip for 1 h at 37°C. After washing away the unbound platelets, the bound platelets were fixed and immunostained for STXBP5 (**A**), P-selectin (**B**) and F-actin using TRITC-phalloidin (**C**). Platelets were additionally stained with anti-STXBP5 antibodies (**E**, **I**, and **M**), anti-tubulin antibodies (**G**, **K**, and **O**) and antibodies against markers for α granules (vWF; **F**), lysosomes (LAMP-1; **J**), and dense granules (CD63; **N**). Images in **A**–**D** were taken using a Zeiss LSM 780 confocal microscope and processed using ZEN blue software, and images in **E**–**P** were taken using a Nikon A1R confocal microscope and processed using NIS-Elements AR 3.2 software; **D**, **H**, **L**, and **P** show 3-color merged views. Scale bars: 10 μm (**A**–**D**); 1 μm (**A**–**D**, insets, and **E**–**P**).

with this area representing the centralized granulomere of an activated platelet. Immunofluorescence staining of STXBP5 in resting platelets, with circumferential tubulin rings, did not show any obvious colocalization with markers for the 3 specific platelet granule types (Figure 3, E–P).

STXBP5 is important for platelet secretion. To explore the functional role of STXBP5, we analyzed *Stxbp5* KO mice. As might be predicted from GWAS analysis (14–19), plasma vWF levels were increased in these mice, although plasma IgG was unaffected, as indicated by light chain levels (Supplemental Figure 1). Platelet extracts from *Stxbp5* KO and littermate WT mice were prepared and subjected to IB analysis. The protein levels of 14 known secretory machinery components were examined; other than STXBP5, none appeared to be significantly altered (Figure 4A). To understand the role of STXBP5, we examined stimulation-dependent release of cargo from all 3 platelet granules: dense granules, α granules, and lysosomes. Secretion of granule cargo from *Stxbp5* KO and WT platelets showed the expected thrombin dose dependence (Figure 4B); however, the percentage release from α granules and lysosome was significantly affected by the loss of STXBP5. The release from dense granules was significantly affected, but to a lesser extent, in this assay system. The kinetics of secretion from

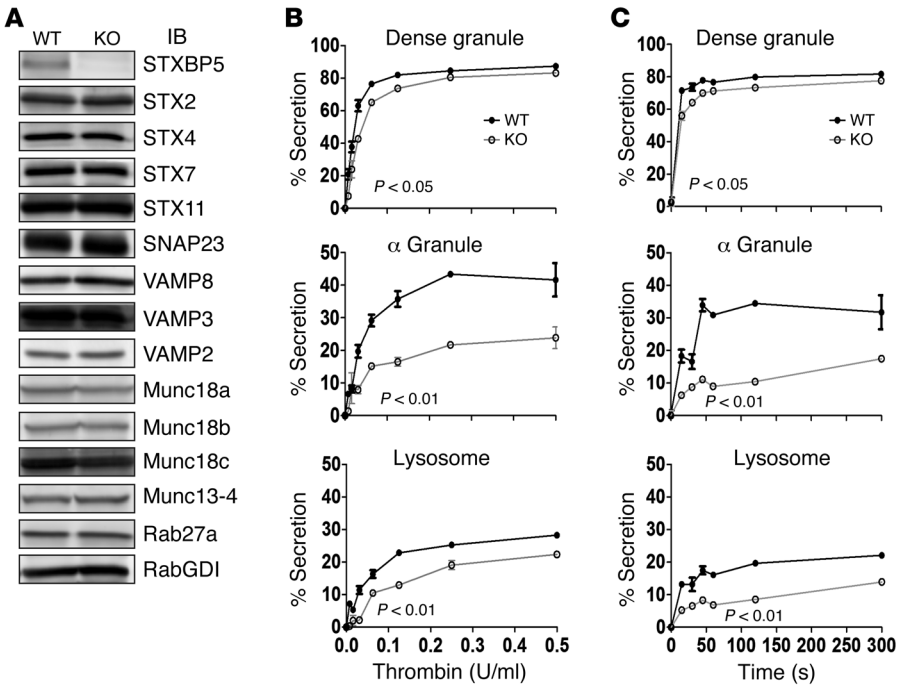

Figure 4. STXBP5-deficient mouse platelets have a secretion defect. (**A**) Platelet extracts (5×10^7 platelets/lane) were prepared from *Stxbp5* KO and WT mice, and the indicated proteins were analyzed by IB. (**B** and **C**) [^{3}H]-Serotonin–labeled platelets from *Stxbp5* KO and WT mice were prepared as described in Methods. Release of [^{3}H]-serotonin from dense granules, PF4 from α granules, and β-hexosaminidase from lysosomes was measured, and percent secretion was calculated. (**B**) Thrombin dose-response experiment; platelets were stimulated for 1 minute. (**C**) Secretion time-course experiment; platelets were stimulated with 0.1 U/ml thrombin. Data are mean ± SEM of triplicate measurements. Significant *P* values (2-way ANOVA) are indicated.

Stxbp5 KO platelets was also significantly defective upon activation with 0.1 U/ml thrombin (Figure 4C).

Because dense granule release is such a rapid process, measuring [^{3}H]-serotonin release in our assay configuration at room temperature (Figure 4, B and C) may not be sufficient to fully appreciate a subtle, albeit significant, kinetic defect. To rectify this, we applied more sensitive lumi-aggregometry to analyze ATP/ADP release from dense granules. ATP/ADP release in response to 100 μM PAR-4, 10 nM A23187, 0.1 μg/ml convulxin, and 0.025, 0.05, and 0.1 U/ml thrombin was substantially inhibited, whereas aggregation was not (Figure 5). Quantification of ATP/ADP release from 3 independent experiments showed significant reductions in *Stxbp5* KO platelets (Figure 5, D and K). To further confirm that STXBP5 is required for α granule and lysosome release, exposure of the respective markers P-selectin and LAMP-1 was analyzed by flow cytometry. Consistently, activation-dependent exposure of both granule membrane markers was reduced approximately 2-fold in *Stxbp5* KO versus WT platelets (Figure 6, A and B).

In agreement with the aggregation data, there was no significant difference in PE-conjugated JonA staining (Figure 6C), which suggests that depletion of STXBP5 did not affect integrin αIIbβ3 activation (15, 44, 45). Electron microscopy (EM) analysis detected no overt morphology differences in *Stxbp5* KO platelets (Supplemental Figure 2). Upon thrombin stimulation, there was similar filopodia formation in both WT and *Stxbp5* KO platelets, which suggests that deficiency of STXBP5 did not affect platelet cytoskeletal rearrangements or platelet activation, but did affect secretion. Additionally, adhesion to fibrinogen was not affected in *Stxbp5* KO platelets, although there was a clear defect in spreading on fibrinogen (Supplemental Figure 3). This is consistent with the role of granule secretion in platelet spreading (46).

STXBP5 is important for platelet granule cargo packaging. As we measured cargo release as a percentage of total, we also detected a decrease in platelet factor 4 (PF4) in *Stxbp5* KO versus WT platelets (Table 1). Serotonin and β-hexosaminidase levels were not significantly reduced; in fact, total serotonin levels and uptake of [^{3}H]-serotonin were increased by approximately 60% (Table 1). These data suggest that STXBP5 contributes to granule biogenesis as well as to secretion. To characterize the effect of STXBP5 loss on platelet cargo, we probed extracts with granule-specific antibodies (Figure 7, A and B). IB data confirmed the reduction of PF4 and showed reduced levels of factor V. Platelet fibrinogen and vWF levels were modestly affected. The total levels of granule membrane proteins (e.g., LAMP-1 and P-selectin) were only slightly affected, while the surface expression of several platelet markers (e.g., GP1bβ, GPVI, and PECAM-1) was largely unaffected (Figure 7, B and C). Consistent with the levels of LAMP-1 and P-selectin, EM analysis showed no significant difference in the number of granules present per platelet section when dense and α granules were counted (Table 1). These data argue that granules are made, but may not be normally loaded with cargo. Further analysis of soluble cargo levels yielded a complex phenotype. Antibody array analysis showed that several cargo proteins were reduced in *Stxbp5* KO platelets. Others were unchanged, and a few, including MMP-9, showed robust increases (Figure 7D). All cargo proteins tested were detectable at some level (Supplemental Figure 4). These data indicate that STXBP5 contributes to the efficacy — and perhaps the selectivity — of granule cargo packaging, but is not essential for the process.

STXBP5 is important for hemostasis. The primary function of platelet secretion is in hemostasis. To assess whether STXBP5 contributes to hemostasis, we used 2 in vivo assays. First, a tail bleeding time assay was performed on 5- to 6-week-old mice. Whereas the 19 WT littermates showed an average bleeding time of 226.4 ± 37.3 s, of the 24 *Stxbp5* KO mice, only 3 had normal bleeding times; the remainder bled excessively until the study was ended at 10 minutes (Figure 8A). The prolonged tail bleed-

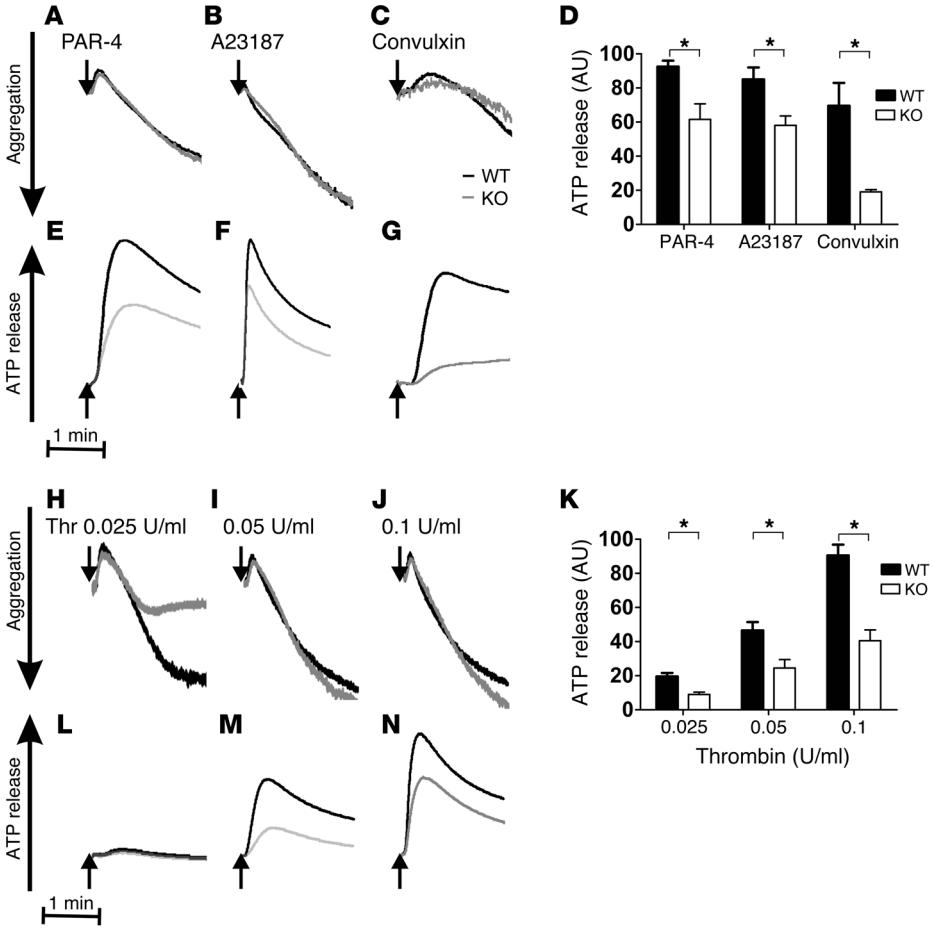

Figure 5. Depletion of STXBP5 in platelets affects ATP/ADP release, but not aggregation. Aggregation (**A**–**C** and **H**–**J**) and ATP/ADP release (**D**–**G** and **K**–**N**) were monitored simultaneously in a lumi-aggregometer. Washed platelets (2.0×10^5/μl) from *Stxbp5* KO and WT mice were stimulated with 100 μM PAR-4 peptide (**A** and **E**), 10 nM A23187 (**B** and **F**), 0.1 μg/ml convulxin (**C** and **G**), or thrombin (Thr) at 0.025 U/ml (**H** and **M**), 0.05 U/ml (**I** and **N**), or 0.1 U/ml (**J** and **O**) for 3 minutes. (**A**–**C**, **E**–**J**, and **L**–**N**) Representative traces from 1 experiment. (**D** and **K**) Mean ± SEM ATP/ADP release from 3 independent experiments. *$P < 0.01$, 2-way ANOVA.

ing of the *Stxbp5* KO mice indicates that STXBP5 is required for hemostasis in this transection injury model.

In agreement with the tail bleeding, there was a robust thrombus formation defect observed in *Stxbp5* KO mice in response to $FeCl_3$ injury of the carotid artery. The average time required to form a stable thrombus in WT littermates was 2.7 ± 0.2 minutes, in contrast to 27.7 ± 2.3 minutes for *Stxbp5* KO mice (Figure 8B), which indicates that STXBP5 is critical for hemostasis in this arterial injury model.

Platelet counts were not significantly different in *Stxbp5* KO and WT littermate mice, although the former exhibited an increase in mean platelet volume (Table 1); therefore, thrombocytopenia is unlikely to be the cause of the bleeding diathesis. The combination of cargo and secretion deficiencies in the *Stxbp5* KO platelets could account for the robust bleeding, but since the mouse strain is a global deletion, other processes could precipitate the hemostatic defects. To address whether the loss of STXBP5 in BM-derived platelets accounted for the hemostatic defect, BM chimeras were constructed via transplantation: *Stxbp5* KO BM was grafted into WT recipients, and vice versa. When *Stxbp5* KO BM was grafted into WT recipients, there was a significant increase in bleeding times in the resulting chimeras compared with WT BM grafted into *Stxbp5* KO recipients (Figure 8C). Similarly, occlusion times in the carotid injury model were significantly prolonged in *Stxbp5* KO BM–grafted WT chimeric mice (Figure 8D). These results suggest that loss of STXBP5 in BM-derived hematopoietic cells (e.g., platelets) contributes to the robust bleeding defect observed (Figure 8, A and B). Since the *Stxbp5* KO animals grafted with WT BM had a normal bleeding profile, it seems unlikely that loss of STXBP5 affects coagulation factors, although this was not directly measured. In summary, these results indicate a role for STXBP5 in platelet granule packaging and secretion and in arterial hemostasis.

Discussion

The novel findings herein were that STXBP5 was required for normal platelet secretion, granule cargo packaging, and hemostasis. This requirement of STXBP5 for platelet exocytosis diverges from the protein's proposed role as a negative regulator in neuronal cell, neuroendocrine cell, and EC secretion (21, 24, 39, 47). Our present data indicate that STXBP5 may be important for cardiovascular health, as echoed in recent GWAS in which *STXBP5* has been linked to thrombosis (14–20).

Platelet granule release requires the secretory machinery components that are universally used for regulated secretion: SNAREs, Munc18, Rabs, and Munc13 (48). Much of the published data suggest that STXBP5 is a negative regulator of secretion, competing with v-SNAREs for t-SNARE binding. As in those prior studies, we showed here that STXBP5 interacted with t-SNARE–containing complexes and that its presence was exclusive of at least 2 platelet v-SNAREs (Figure 2). However, deletion of STXBP5, as well as inclusion of an anti-STXBP5 antibody into

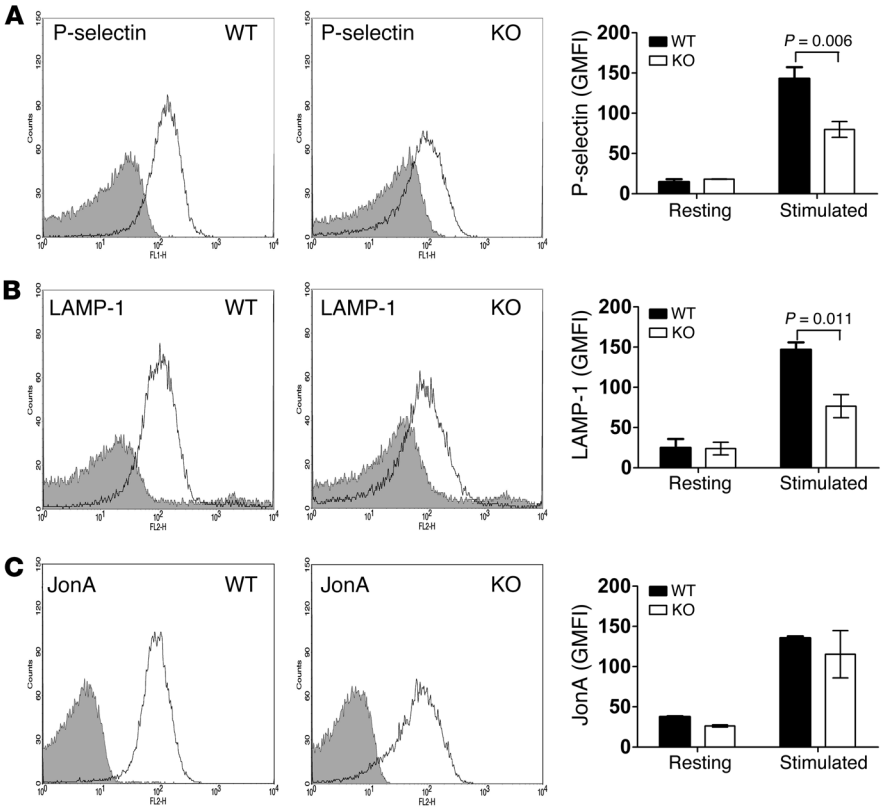

Figure 6. Deletion of STXBP5 inhibits P-selectin and LAMP-1 exposure, but not integrin activation. Washed platelets (2×10^6) from *Stxbp5* KO and WT mice were stimulated with or without 0.1 U/ml thrombin for 1 minute and then incubated with FITC-conjugated anti–P-selectin (**A**), FITC-conjugated LAMP-1 (**B**), or PE-conjugated JonA (**C**) Abs for 15 minutes at room temperature. Fluorescence intensities were measured by flow cytometry. Shown are representative data (black lines, resting; gray lines, stimulated) and geometric MFI (mean ± SEM) of 3 independent experiments. Significant *P* values (2-way ANOVA) are indicated.

a permeabilized platelet secretion assay, inhibited rather than enhanced platelet secretion (Figures 4–6 and Supplemental Figure 5). This result raises the question of how STXBP5 could have a positive effect on exocytosis. Studies in *Drosophila* show that loss of STXBP5 prolongs the excitatory junctional currents (EJCs) at neuromuscular junctions (NMJs) (49). This could be due to ectopic vesicle priming (adjacent to active zones) or prolonged fusion pore opening, which suggests that the role of STXBP5 is to spatially restrict vesicle priming and/or fusion. In platelets, spatial granule priming for exocytosis may be critical for efficacious secretion. While our in-suspension secretion assays (Figures 4–6) may be less influenced by a loss of polarization, secretion in a forming thrombus almost assuredly needs to be polarized (50). Thus, STXBP5 may be important for normal thrombosis, and its deletion would cause the hemostasis defects we observed (Figure 8). At this stage, it is unclear why STXBP5 is important for secretion from yeast (25), INS-1E cells (35), or platelets (Figures 4–6); however, its interactions with cytoskeleton (Figure 2E and Figure 3), especially myosin Va (28, 42, 51), may hint at a role in spatially coordinating SNARE complexes for membrane fusion and subsequent secretion. STXBP5 interactions with cytoskeleton could contribute to granule biogenesis by directing the trafficking of cargo proteins to α granules forming in megakaryocytes. The heterogeneity in cargo levels we observed herein (Figure 7 and Supplemental Figure 4) may be indicative of multiple pathways for granule cargo sorting and packaging. Further work will be required to address these potential functions of STXBP5.

GWAS have linked SNPs in *STXBP5* to alterations in vWF levels (14–19) and tPA levels (18). Loss of STXBP5 increases vWF release from ECs (47), but decreases tPA release (20). These results highlight potentially conflicting roles for STXBP5 in ECs, which may relate to which granules are being released. vWF and tPA are enriched in different granules in ECs (52). Combining these 2 effects, heightened vWF and decreased tPA, might be expected to increase thrombotic risk, consistent with the premise of the GWAS. Conversely, an SNP encoding a nonsynonymous substitution in *STXBP5* (N436S) has been linked to increased bleeding in a female population homozygous for the allele (18). The dramatically prolonged bleeding times in the tail transection model and the hemostasis defects in the $FeCl_3$-induced carotid artery injury model we observed in *Stxbp5* KO mice and in *Stxbp5* KO BM–grafted WT mice are consistent with this prior report and support a connection between STXBP5 and bleeding risk. At this

Table 1. Properties of WT and *Stxbp5* KO mouse platelets

	WT	*Stxbp5* KO	*P*
Platelet count (×1,000/μl)	824 ± 123	881 ± 101	0.561
Mean platelet volume (fl)	4.20 ± 0.23	6.28 ± 0.10	0.001
Serotonin (μM/10^8 platelets)[A]	6.31 ± 0.5	10.64 ± 1.4	0.006
^{3}[H]-Serotonin uptake (cpm/10^8 platelets)	2,515 ± 224	4,101 ± 545	0.036
PF4 (pg/10^6 platelets)	1,690 ± 120	545.5 ± 15	<0.0001
β-Hexosaminidase (nMh^{-1}/10^6 platelets)	54 ± 10	57 ± 11	0.878
Dense granules/platelet[B]	0.46 ± 0.57	0.52 ± 0.57	0.320
α Granules/platelet[B]	7.97 ± 1.80	7.84 ±1.22	0.453

P values were calculated using Student's *t* test. [A]Determined using the fluorescence *o*-phthalaldehyde assay (see Supplemental Methods). [B]Granules in each platelet in an EM section were counted (*n* = 200 platelets counted).

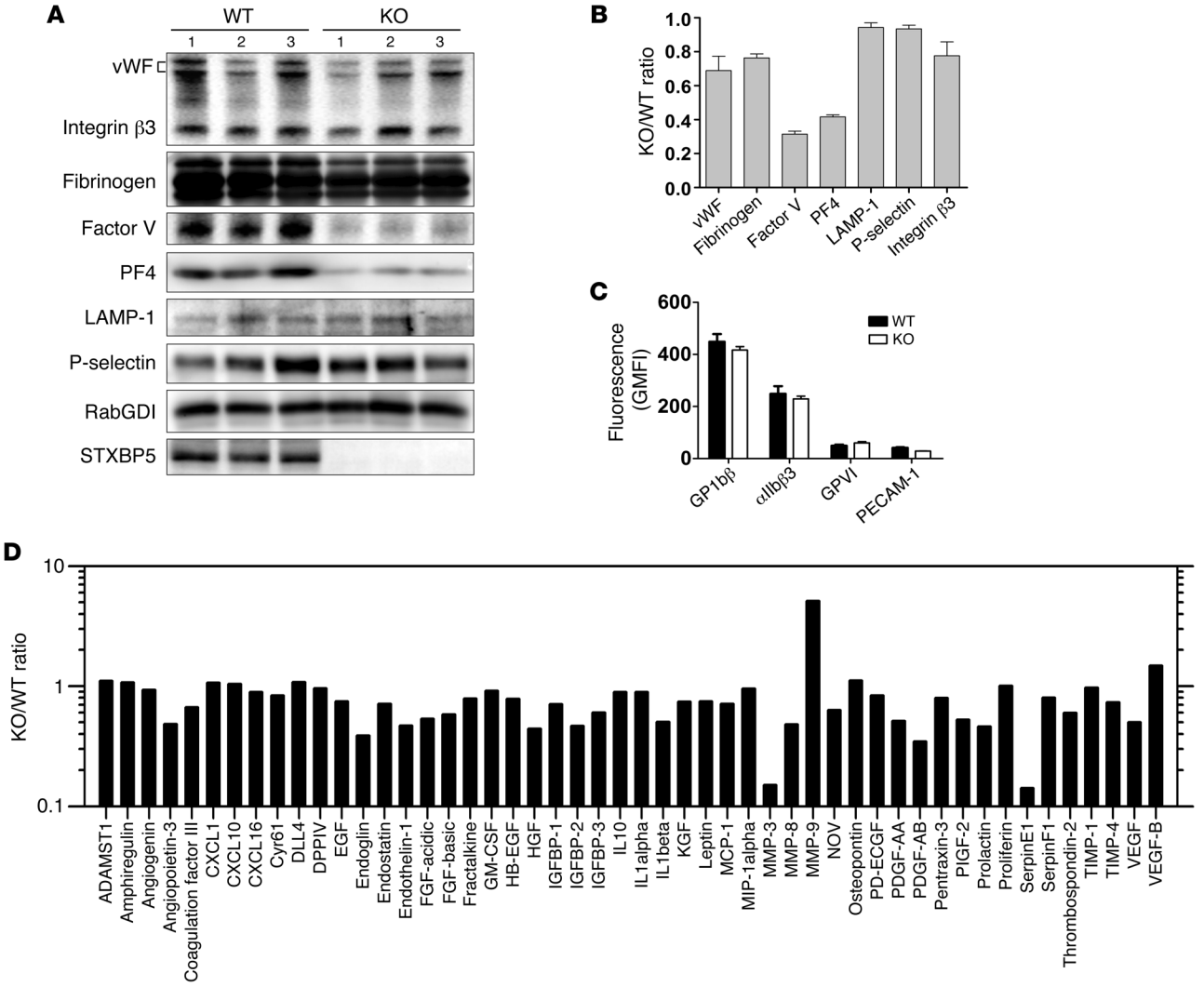

Figure 7. STXBP5-deficient mouse platelets have a complex granule cargo defect. (**A** and **B**) Platelet extracts (5×10^7 platelets/lane) were prepared from 3 individual *Stxbp5* KO or WT mice. The indicated proteins were analyzed by IB (**A**) and quantified with Image Lab 4.0.1 or ImageQuant TL. After normalization using RabGDI as loading control, the *Stxbp5* KO/WT ratio was calculated (**B**). (**C**) Washed platelets (2×10^6) from 3 individual *Stxbp5* KO or WT mice were incubated with FITC-conjugated anti-GP1bβ, anti-αIIbβ3, anti-GPVI, or anti–PECAM-1 for 15 minutes at room temperature. Geometric MFI (mean ± SEM) was determined using flow cytometry. (**D**) Antibody array analysis of platelet extracts. Extracts were prepared from WT or *Stxbp5* KO mice and probed using duplicate Proteome Profiler Mouse Angiogenesis Antibody Arrays (see Methods). The fluorescence intensity from 2 experiments was used to calculate a *Stxbp5* KO/WT ratio for each protein detected on the array. The average of the 2 calculated ratios is plotted. Note that the *y* axis is a log scale. SDF-1, PF4, and angiopoietin 1 were excluded from analysis due to saturation of their respective spots on the array membranes.

stage, it is unclear whether the N436S substitution has any effect on STXBP5 stability or function.

Zhu et al. have shown that loss of STXBP5 enhances EC secretion of vWF and increases platelet binding to activated ECs (47). Consistent with our results (Supplemental Figure 1), Zhu et al. showed significantly increased plasma vWF levels in *Stxbp5* KO mice (47). Clearly, the increased vWF is not sufficient to offset the platelet secretion defect described herein, since we observed bleeding tendencies in the 2 arterial hemostasis models tested (Figure 8). However, venous thrombi are mainly composed of fibrin and red blood cells, whereas arterial thrombi are dominated by platelets and fibrin; therefore, it is possible that STXBP5-mediated platelet secretion is more important for arterial hemostasis. It remains to be determined how the loss of STXBP5 affects venous thrombosis.

In summary, our data provide a potential explanation for the GWAS (14–19) linking STXBP5 with cardiovascular disease risk. Our findings showed that STXBP5 was present in platelets and was important for cargo release from dense granules, α granules, and lysosomes as well as for packaging of some cargo into granules. Mice with platelets deficient in STXBP5 displayed robust defects in thrombus formation in 2 arterial hemostasis models, consistent with the granule biogenesis and release defects. Our data add another component to the pathway of protein-protein interactions that culminates in platelet secretion. They also suggest that platelets may be a useful system for understanding how STXBP5 positively affects exocytosis in other systems, perhaps through its associations with cytoskeleton. Moreover, platelet STXBP5 may be a useful diagnostic marker for cardiovascular diseases.

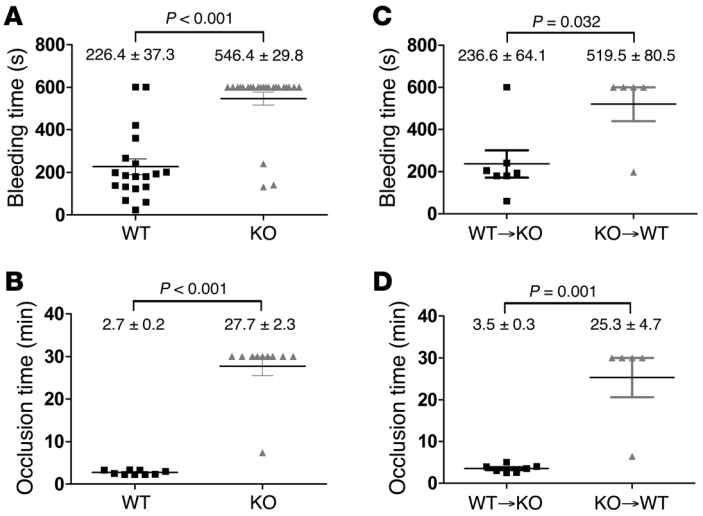

Figure 8. Hemostasis and thrombus formation are impaired in STXBP5-deficient mice. (**A**) Tail bleeding times were measured after tail transection from *Stxbp5* KO (n = 24) and WT (n = 19) littermates. (**B**) Thrombus formation in the carotid artery was induced by topical application of 5% $FeCl_3$, and blood flow was monitored from *Stxbp5* KO (n = 10) and WT (n = 9) littermates. (**C** and **D**) Chimeric mice (WT BM transplanted into *Stxbp5* KO littermates [WT→KO], n = 7; *Stxbp5* KO BM transplanted into WT littermates [KO→WT], n = 5) were analyzed using the same assays. Tail bleeding times (**C**) and the time to blood flow cessation from 5% $FeCl_3$-induced carotid thrombosis (**D**) were measured. Each symbol represents an individual mouse; mean ± SEM are noted. P values (log-rank test) are indicated.

Methods

Antibodies and reagents. Anti-STXBP5 mAb (611296), anti-Rab27a mAb (clone 20.1), anti-PECAM, FITC-conjugated anti-mouse P-selectin, and unconjugated anti-mouse P-selectin were from BD Biosciences. A rabbit anti-STXBP5 polyclonal Ab (HPA039991) was from Atlas Antibodies. The anti–hLAMP-1 (H4A3) and anti-hCD63 (H5C6) mAbs were from the University of Iowa Developmental Studies Hybridoma Bank. Anti-Munc18b (sc-14563) polyclonal Ab was from Santa Cruz. Antibodies against STX2, STX4, STX7, SNAP23, VAMP8, Munc18c, Rab-GDI, VAMP2 (synaptobrevin), VAMP3 (cellubrevin), VAMP7, VAMP8 (endobrevin), and Munc13-4 were as described previously (6, 8, 53). Anti-STX11 polyclonal Ab and anti-Munc18a mAb (clone 131.1) were purchased from Synaptic System GmbH. PE-conjugated JonA mAb, anti-GP1bβ, and anti GPVI Abs were purchased from Emfret Analytics. Anti-human fibrinogen and anti-vWF polyclonal Abs were from Dako. The anti–integrin β3 antibody and the Alexa Fluor 647–labeled rabbit anti–α-tubulin antibody (11H10) were from Cell Signaling. The anti–factor V antibody was provided by B. Bouchard (University of Vermont, Burlington, Vermont, USA). A STXBP5 expression vector (provided by U. Ashery, Tel Aviv University, Tel Aviv, Israel) was used to make antigens for the production and purification of a polyclonal anti-STXBP5 antibody (see Supplemental Methods). Anti–β-actin antibody and alkaline phosphatase–conjugated anti-IgGs were from Sigma-Aldrich. Protein A–conjugated sepharose, 2-methyl-2-butanol, 2,2,2 tribromoethanol (Avertin), and $FeCl_3$ were from Sigma-Aldrich. The rest of the materials used in this study were of reagent grade.

Protein production. Expression plasmids to create complexes of full-length human SNAP23, Munc18a, and Munc18c and the cytoplasmic domains of human STX2 (aa 1–251) and STX4 (aa 1–265) were constructed using pRSFDuet-1 (Novagen) and confirmed by DNA sequencing. All syntaxin-containing complexes were expressed in *E. coli* and purified using Ni^{2+}-NTA (6) and S-protein (Novagen) affinity chromatography.

RT-PCR. Identification of STXBP5 isoforms was performed as described previously (29, 40), with slight modification. Human platelets were isolated from banked, platelet-rich plasma (13), total RNA was isolated using QIAamp RNA Blood Mini Kit (QIAGEN), and cDNA was synthesized using TaqMan Reverse Transcription Reagents Kit (Applied Biosystems). PCR amplification was performed using primers specific for the b-STXBP5 (5′-CTCCGACTTCCGGTTCTTCCTC-3′ and 5′-TTCAGCGTGATGACAAAGGC-3′), m-STXBP5 (5′-CTCCGACTTCCGCAAAGATGTC-3′ and 5′-TTCAGCGTGATGACAAAGGC-3′), and s-STXBP5 (5′-CTCCGACTTCCGATGTGAAAG-3′ and 5′-TTCAGCGTGATGACAAAGGC-3′) isoforms (29, 40).

Immunoprecipitation of STXBP5-interacting proteins. Washed platelet suspensions (10^9 platelets) were lysed with equal volumes of 2× lysis buffer (100 mM HEPES/KOH, pH 7.4; 2% Triton X-100; 2 mM EGTA; 2 mM EDTA; 150 mM NaCl; and 2× protease inhibitor cocktail) on ice for 30 minutes. The lysates were clarified by centrifugation, and the supernatants were precleared with protein G/A sepharose (GE Healthcare). The interacting proteins were immunoprecipitated with anti-STXBP5, anti-Munc18b, or anti–Munc13-4 Abs, followed by incubation with protein G sepharose. The immunoprecipitates were recovered by centrifugation, washed with lysis buffer, and analyzed by SDS-PAGE and IB.

Genotyping of Stxbp5 KO mice. *Stxbp5* KO mice on a 50% 129Sv, 25% C57BL/6, and 25% DBA/2 background were generated as previously described (32). Heterozygous embryos of *Stxbp5* KO mice were recovered into live mice by the Jackson Laboratory. Genotype was determined by PCR using DNA isolated from tail tip biopsies. The primers used were as follows: *Stxbp5* KO forward, 5′-GGGCGCCCGGTTCTTTTTGTC-3′; *Stxbp5* KO reverse, 5′-GCCATGATGGATACTTTCTCG-3′; WT forward, 5′-TTCTGCTCCCCGCTGCTCCTT-3′; WT reverse, 5′-TCCCCGCTCCCTTCACCTTGC-3′. PCR products were 224 bp for the *Stxbp5* KO allele and 300 bp for the WT allele.

Measurement of secretion from intact platelets. The secretion assay was carried out as described previously (13); see Supplemental Methods for details. Briefly, washed platelets were labeled with [^{3}H]-serotonin (0.4 μCi/ml) for 1 hour at 37°C. After washing with HEPES/Tyrode buffer (10 mM HEPES/NaOH, pH 7.4; 5.56 mM glucose; 137 mM NaCl; 12 mM $NaHCO_3$; 2.7 mM KCl; 0.36 mM KH_2PO_4; and 1 mM $MgCl_2$) in the presence of 0.2 U/ml apyrase, the platelets were resuspended and adjusted to 2.5×10^5/μl. For titration experiments, the indicated concentrations of thrombin were added, and the reactions were stopped at 1 minute with a 2-fold excess of hirudin. For time course experiments, 0.1 U/ml thrombin was added for the indicated times, and reactions were stopped with hirudin. Supernatants and pellets were recovered after centrifugation at 13,000 *g* for

1 minute, and the pellets were lysed with an equal volume of lysis buffer (PBS, pH 7.4, and 1% Triton X-100) for 1 hour on ice. Both supernatants and pellets were assayed for 3 granule cargo markers: [^{3}H]-serotonin for dense granules by scintillation counting, platelet factor 4 (PF4) for α granules by ELISA, and β-hexosaminidase for lysosomes by colorimetric assay using *p*-nitrophenyl-*N*-acetyl-β-D-glucosaminide, as previously described (54). Secretion was then calculated as (supernatant/[supernatant + pellet]) and expressed as a percentage; the analysis yields a measurement of total cargo content (supernatant plus pellet) and allows for assessment of secretion efficacy independent of cargo content.

Immunofluorescence microscopy. Platelet preparation and immunostaining were performed as previously described (55), with slight modification. Briefly, sterile glass coverslips were coated with 50 μg/ml human fibrinogen for 24 hours at 4°C. Washed platelets were placed onto fibrinogen-coated coverslips for 1 hour at 37°C. Platelets were fixed with 4% paraformaldehyde for 15 minutes and quenched with 50 mM NH_4Cl. Cells were rinsed with 10% FBS/PBS and incubated with the indicated primary antibodies in 10% FBS/PBS containing 0.2% saponin O/N at 4°C. After washing with 10% FBS/PBS, cells were incubated with the appropriate fluorophore-conjugated anti-IgG secondary antibody for 2 hours. After washing, some samples were incubated with TRITC-conjugated phalloidin in 10% FBS/PBS with 0.2% saponin. Coverslips were mounted and examined with a LSM 780 confocal microscope (Carl Zeiss), and images were processed using ZEN blue software (Carl Zeiss). Additional imaging was done using a Nikon A1R confocal microscope, and images were processed using NIS-Elements AR 3.2 software (Nikon).

Platelet aggregation and ATP/ADP release. Murine platelets (2.5×10^5/μl) were prepared (13), recalcified with 0.7 mM $CaCl_2$, placed into siliconized cuvettes, and stirred for 3 minutes at 37°C at 1,200 rpm. Luciferin-luciferase substrate was added, followed by the indicated agonists, and the percent change in light transmission was measured. Aggregation and ATP/ADP secretion were monitored using a Model 460VS Lumi-Dual-aggregometer, and traces were acquired using a Model 810 Aggro/Link interface with Aggro/Link software (all from Chrono-Log).

Flow cytometry analysis. Washed murine platelets (2×10^6) were kept as resting or were stimulated with thrombin (0.1 U/ml) for 1 minute, after which the reaction was stopped with hirudin. After incubation with antibodies (5 μl) for 15 minutes at room temperature, the reactions were diluted 10-fold with HEPES/Tyrode buffer (pH 6.5). The samples were transferred to tubes, and fluorescence intensities were measured using a FACScan flow cytometer and analyzed using CellQuest (BD Biosciences).

Tail bleeding assay. Tail vein bleeding times were determined as previously described (56). Briefly, 5- to 6-week-old mice were anesthetized with ketamine (75 mg/kg i.p.). Tails were transected 3 mm from the tip and immersed in saline at 37°C. The time from incision to bleeding cessation was recorded. Animals were observed for an additional minute to assess rebleeding. Prolonged bleeding was stopped manually after 10 minutes. Statistical analysis was performed using the log-rank test (GraphPad Prism 5).

$FeCl_3$-induced arterial hemostasis model. The $FeCl_3$-induced arterial thrombosis model was as previously described (57). Briefly, mice 8–12 weeks of age were anesthetized with Avertin (0.2 g/kg i.p.) and placed on a 37°C heating pad. The left carotid artery was exposed, and a Doppler TS420 flowmeter (0.5VB; Transonic System Inc.) was placed on the artery to monitor blood flow. Thrombus formation was induced by placing a small piece of filter paper, saturated with 5% $FeCl_3$ solution, on the vessel for 3 minutes. Time from application to cessation of flow was measured. Experiments were terminated at 30 minutes. Statistical analysis was performed using the log-rank test (GraphPad Prism 5).

BM transplantation mouse model. BM transplantation was performed as previously described (58), with some modification. Briefly, BM harvested from femurs and tibias of 6-week-old WT or *Stxbp5* KO mice was resuspended with 10 mM HEPES, pH 7.4 buffer containing 25 U/ml heparin and 5% FBS and adjusted to 5×10^7 cells/ml. The cell suspension (0.1 ml) was injected into the retroorbital sinus of lethally irradiated mice. After 6 weeks of recovery, tail bleeding and $FeCl_3$-induced hemostasis assays were performed. Statistical analysis was performed using the log-rank test (GraphPad Prism 5).

Subcellular fractionation of platelets. Human platelets were resuspended in HEPES/Tyrode buffer (pH 7.4) and treated with or without 0.1 U/ml thrombin for 5 minutes. The resting and activated platelets were disrupted by 5 freeze-thaw cycles. After disruption, the unbroken cells were removed by centrifugation at 700 *g* for 5 minutes, and the supernatants were fractionated by ultracentrifugation at 100,000 *g* for 1 hour. The supernatant (cytosol) was collected, and the resulting pellets were solublized with 1% Triton X-100, incubated on ice for 15 minutes, and then subjected to centrifugation at 100,000 *g* for 1 hour. The supernatant (Triton X-100–soluble fraction) was collected, and the resulting pellets were solublized with 1% *n*-octyl-β-D-glucopyranoside, incubated on ice for 15 minutes, and then subjected to centrifugation at 100,000 *g* for 1 hour. The supernatant (*n*-octyl-β-D-glucopyranoside–soluble fraction) was collected. The detergent-insoluble pellets were solublized in SDS-PAGE loading buffer. The supernatants (soluble fractions) and pellets (detergent-insoluble fractions) were probed by IB using anti-STXBP5, anti-RabGDI, anti-STX4, anti-SNAP23, and anti–β-actin antibodies.

Angiogenesis antibody array analysis of platelet granule cargo. Proteome Profiler Mouse Angiogenesis Antibody Array (ARY 015; R&D Systems) was used according to the manufacturer's instructions. Briefly, the nitrocellulose membranes were first incubated in blocking buffer for 1 hour. Platelet extracts (from 10^8 platelets) were prepared in 1 ml lysis buffer (1% NP-40; 20 mM Tris-HCl, pH 8.0; 137 mM NaCl; 10% glycerol; 2 mM EDTA; and 10× protease inhibitor cocktail) and mixed with a cocktail of biotin-labeled detection antibodies against different individual angiogenesis-related proteins. After incubation for 1 hour, the mixture of the platelet sample and detection antibodies was then incubated with the nitrocellulose membranes O/N at 4°C. The membranes were washed 3 times and incubated with HRP-conjugated streptavidin for 30 minutes. After washing the membranes 3 times, the signals for each array spot were detected with Supersignal ELISA Femto Maximum Sensitivity Substrate (Thermo-Scientific) using a ChemiDoc MP System (BioRad). The array experiments were run in duplicate. Fluorescence intensities for each spot were measured, background was subtracted, and the *Stxbp5* KO/WT ratio was calculated and plotted using SigmaPlot (version 12.0; Systat Software Inc.). Under these conditions, spots for 3 proteins — SDF-1, PF4, and angiopoietin 1 — were saturated, and thus failed to yield quantitative data (Supplemental Figure 4). These were excluded from analysis.

Statistics. Data from bleeding time and occlusion assays were analyzed by log-rank test. Data from secretion assays and FACS-based

experiments were analyzed by 2-way ANOVA. A 1-tailed Student's *t* test was used to analyze the properties of platelets from *Stxbp5* KO and WT mice. A *P* value less than 0.05 was considered significant.

Study approval. Animal procedures were approved by the IACUC of University of Kentucky. Human samples were from anonymized units; thus, no IRB approval or informed consent was required.

Acknowledgments

We thank Uri Ashery for providing a STXBP5 expression construct, Beth Bouchard for anti–factor V antibody, Mary Gail Engle and Jim Begley (Imaging Facility of University of Kentucky) for help with EM analysis, Greg Bauman (Flow Cytometry Core Facility of University of Kentucky) for help with FACS analysis, the staff of the Department of Laboratory Animal Resources at University of Kentucky for assistance, Richard Charnigo (Department of Statistics, University of Kentucky) for help with data analysis, Leighton Izu (University of California, Davis, California, USA) for insightful discussions, the staff of the Kentucky Blood Center for support, and the members of the Whiteheart laboratory for comments and careful proofreading of the manuscript. The mass spectrometry analysis was performed by Carol Beach at the University of Kentucky Center for Structural Biology Protein Core Facility; this core and the imaging facility are supported in part by funds from NIH National Center for Research Resources (NCRR) grant P20 RR020171. This work is supported by NIH grants HL56652 and HL082193 to S.W. Whiteheart and NIH grant T32HL091812 to S. Ye.

Address correspondence to: Sidney W. Whiteheart, Department of Molecular and Cellular Biochemistry, University of Kentucky College of Medicine, 741 South Limestone, Biomedical Biological Sciences Research Building, Lexington, Kentucky 40536-0509, USA. Phone: 859.257.4882; E-mail: whitehe@uky.edu.

1. Michelson AD. Antiplatelet therapies for the treatment of cardiovascular disease. *Nat Rev Drug Discov*. 2010;9(2):154–169.
2. Lopes RD. Antiplatelet agents in cardiovascular disease. *J Thromb Thrombolysis*. 2011; 31(3):306–309.
3. Michelson AD. *Platelets*. San Diego, California, USA: Elservier Science; 2002.
4. Graham GJ, Ren Q, Dilks JR, Blair P, Whiteheart SW, Flaumenhaft R. Endobrevin/VAMP-8-dependent dense granule release mediates thrombus formation in vivo. *Blood*. 2009;114(5):1083–1090.
5. Weber T, et al. SNAREpins: minimal machinery for membrane fusion. *Cell*. 1998;92(6):759–772.
6. Chen D, Bernstein AM, Lemons PP, Whiteheart SW. Molecular mechanisms of platelet exocytosis: role of SNAP-23 and syntaxin 2 in dense core granule release. *Blood*. 2000;95(3):921–929.
7. Chen D, Lemons PP, Schraw T, Whiteheart SW. Molecular mechanisms of platelet exocytosis: role of SNAP-23 and syntaxin 2 and 4 in lysosome release. *Blood*. 2000;96(5):1782–1788.
8. Bryceson YT, et al. Defective cytotoxic lymphocyte degranulation in syntaxin-11 deficient familial hemophagocytic lymphohistiocytosis 4 (FHL4) patients. *Blood*. 2007;110(6):1906–1915.
9. Ye S, Karim ZA, Al Hawas R, Pessin JE, Filipovich AH, Whiteheart SW. Syntaxin-11, but not syntaxin-2 or syntaxin-4, is required for platelet secretion. *Blood*. 2012;120(12):2484–2492.
10. Sudhof TC, Rothman JE. Membrane fusion: grappling with SNARE and SM proteins. *Science*. 2009;323(5913):474–477.
11. Paumet F, Rahimian V, Rothman JE. The specificity of SNARE-dependent fusion is encoded in the SNARE motif. *Proc Natl Acad Sci U S A*. 2004;101(10):3376–3380.
12. Tolmachova T, Abrink M, Futter CE, Authi KS, Seabra MC. Rab27b regulates number and secretion of platelet dense granules. *Proc Natl Acad Sci U S A*. 2007;104(14):5872–5877.
13. Al Hawas R, Ren Q, Ye S, Karim ZA, Filipovich AH, Whiteheart SW. Munc18b/STXBP2 is required for platelet secretion. *Blood*. 2012;120(12):2493–2500.
14. Antoni G, et al. Combined analysis of three genome-wide association studies on vWF and FVIII plasma levels. *BMC Med Genet*. 2011;12:102.
15. Campos M, et al. Genetic determinants of plasma von Willebrand factor antigen levels: a target gene SNP and haplotype analysis of ARIC cohort. *Blood*. 2011;117(19):5224–5230.
16. Smith NL, et al. Genetic variation associated with plasma von Willebrand factor levels and the risk of incident venous thrombosis. *Blood*. 2011;117(22):6007–6011.
17. Smith NL, et al. Novel associations of multiple genetic loci with plasma levels of factor VII, factor VIII, and von Willebrand factor: The CHARGE (Cohorts for Heart and Aging Research in Genome Epidemiology) Consortium. *Circulation*. 2010;121(12):1382–1392.
18. van Loon JE, Sanders YV, de Wee EM, Kruip MJ, de Maat MP, Leebeek FW. Effect of genetic variation in STXBP5 and STX2 on von Willebrand factor and bleeding phenotype in type 1 von Willebrand disease patients. *PLoS One*. 2012;7(7):e40624.
19. van Loon JE, et al. Effect of genetic variations in syntaxin-binding protein-5 and syntaxin-2 on von Willebrand factor concentration and cardiovascular risk. *Circ Cardiovasc Genet*. 2010;3(6):507–512.
20. Huang J, et al. Genome-wide association study for circulating tissue plasminogen activator levels and functional follow-up implicates endothelial STXBP5 and STX2. *Arterioscler Thromb Vasc Biol*. 2014;34(5):1093–1101.
21. Fujita Y, et al. Tomosyn: a syntaxin-1-binding protein that forms a novel complex in the neurotransmitter release process. *Neuron*. 1998;20(5):905–915.
22. Widberg CH, Bryant NJ, Girotti M, Rea S, James DE. Tomosyn interacts with the t-SNAREs syntaxin4 and SNAP23 and plays a role in insulin-stimulated GLUT4 translocation. *J Biol Chem*. 2003;278(37):35093–35101.
23. Scales SJ, Hesser BA, Masuda ES, Scheller RH. Amisyn, a novel syntaxin-binding protein that may regulate SNARE complex assembly. *J Biol Chem*. 2002;277(31):28271–28279.
24. Ashery U, Bielopolski N, Barak B, Yizhar O. Friends and foes in synaptic transmission: the role of tomosyn in vesicle priming. *Trends Neurosci*. 2009;32(5):275–282.
25. Lehman K, Rossi G, Adamo JE, Brennwald P. Yeast homologues of tomosyn and lethal giant larvae function in exocytosis and are associated with the plasma membrane SNARE, Sec9. *J Cell Biol*. 1999;146(1):125–140.
26. Gracheva EO, Burdina AO, Touroutine D, Berthelot-Grosjean M, Parekh H, Richmond JE. Tomosyn negatively regulates both synaptic transmitter and neuropeptide release at the C. elegans neuromuscular junction. *J Physiol*. 2007;585(pt 3):705–709.
27. Strand D, et al. The Drosophila lethal(2)giant larvae tumor suppressor protein forms homo-oligomers and is associated with nonmuscle myosin II heavy chain. *J Cell Biol*. 1994;127(5):1361–1373.
28. Pruyne DW, Schott DH, Bretscher A. Tropomyosin-containing actin cables direct the Myo2p-dependent polarized delivery of secretory vesicles in budding yeast. *J Cell Biol*. 1998;143(7):1931–1945.
29. Yokoyama S, Shirataki H, Sakisaka T, Takai Y. Three splicing variants of tomosyn and identification of their syntaxin-binding region. *Biochem Biophys Res Commun*. 1999;256(1):218–222.
30. Groffen AJ, Jacobsen L, Schut D, Verhage M. Two distinct genes drive expression of seven tomosyn isoforms in the mammalian brain, sharing a conserved structure with a unique variable domain. *J Neurochem*. 2005;92(3):554–568.
31. Hatsuzawa K, Lang T, Fasshauer D, Bruns D, Jahn R. The R-SNARE motif of tomosyn forms SNARE core complexes with syntaxin 1 and SNAP-25 and down-regulates exocytosis. *J Biol Chem*. 2003;278(33):31159–31166.
32. Sakisaka T, et al. Dual inhibition of SNARE complex formation by tomosyn ensures controlled neurotransmitter release. *J Cell Biol*. 2008;183(2):323–337.
33. Yizhar O, et al. Multiple functional domains are involved in tomosyn regulation of exocytosis. *J Neurochem*. 2007;103(2):604–616.
34. Baba T, Sakisaka T, Mochida S, Takai Y. PKA-catalyzed phosphorylation of tomosyn and its implication in Ca2+-dependent exocytosis of neurotransmitter. *J Cell Biol*. 2005;170(7):1113–1125.
35. Cheviet S, et al. Tomosyn-1 is involved in a post-docking event required for pancreatic beta-cell

exocytosis. *J Cell Sci*. 2006;119(pt 14):2912–2920.
36. Davis LK, et al. Novel copy number variants in children with autism and additional developmental anomalies. *J Neurodev Disord*. 2009;1(4):292–301.
37. Sandrock K, Nakamura L, Vraetz T, Beutel K, Ehl S, Zieger B. Platelet secretion defect in patients with familial hemophagocytic lymphohistiocytosis type 5 (FHL-5). *Blood*. 2010;116(26):6148–6150.
38. Hampson A, O'Connor A, Smolenski A. Synaptotagmin-like protein 4 and Rab8 interact and increase dense granule release in platelets. *J Thromb Haemost*. 2013;11(1):161–168.
39. Yizhar O, et al. Tomosyn inhibits priming of large dense-core vesicles in a calcium-dependent manner. *Proc Natl Acad Sci U S A*. 2004;101(8):2578–2583.
40. Zhang W, et al. Tomosyn is expressed in beta-cells and negatively regulates insulin exocytosis. *Diabetes*. 2006;55(3):574–581.
41. Burkhart JM, Schumbrutzki C, Wortelkamp S, Sickmann A, Zahedi RP. Systematic and quantitative comparison of digest efficiency and specificity reveals the impact of trypsin quality on MS-based proteomics. *J Proteomics*. 2012;75(4):1454–1462.
42. Rowley JW, et al. Genome-wide RNA-seq analysis of human and mouse platelet transcriptomes. *Blood*. 2011;118(14):e101–e111.
43. Falet H, Hoffmeister KM, Neujahr R, Hartwig JH. Normal Arp2/3 complex activation in platelets lacking WASp. *Blood*. 2002;100(6):2113–2122.
44. Bergmeier W, Stefanini L. Novel molecules in calcium signaling in platelets. *J Thromb Haemost*. 2009;7(suppl 1):187–190.
45. Buensuceso CS, Arias-Salgado EG, Shattil SJ. Protein-protein interactions in platelet alphaI-Ibbeta3 signaling. *Semin Thromb Hemost*. 2004;30(4):427–439.
46. Peters CG, Michelson AD, Flaumenhaft R. Granule exocytosis is required for platelet spreading: differential sorting of α-granules expressing VAMP-7. *Blood*. 2012;120(1):199–206.
47. Zhu Q, et al. Syntaxin-binding protein STXBP5 inhibits endothelial exocytosis and promotes platelet secretion. *J Clin Invest*. 2014;124(10):4503–4516.
48. Sudhof TC, Rizo J. Synaptic vesicle exocytosis. *Cold Spring Harb Perspect Biol*. 2011;3(12):a005637.
49. Chen K, Richlitzki A, Featherstone DE, Schwarzel M, Richmond JE. Tomosyn-dependent regulation of synaptic transmission is required for a late phase of associative odor memory. *Proc Natl Acad Sci U S A*. 2011;108(45):18482–18487.
50. Brass LF, Tomaiuolo M, Stalker TJ. Harnessing the platelet signaling network to produce an optimal hemostatic response. *Hematol Oncol Clin North Am*. 2013;27(3):381–409.
51. Pastural E, et al. Griscelli disease maps to chromosome 15q21 and is associated with mutations in the myosin-Va gene. *Nat Genet*. 1997;16(3):289–292.
52. Knipe L, et al. A revised model for the secretion of tPA and cytokines from cultured endothelial cells. *Blood*. 2010;116(12):2183–2191.
53. Schraw TD, Lemons PP, Dean WL, Whiteheart SW. A role for Sec1/Munc18 proteins in platelet exocytosis. *Biochem J*. 2003;374(pt 1):207–217.
54. Schraw TD, et al. Granule stores from cellubrevin/VAMP-3 null mouse platelets exhibit normal stimulus-induced release. *Blood*. 2003;102(5):1716–1722.
55. Choi W, Karim ZA, Whiteheart SW. Arf6 plays an early role in platelet activation by collagen and convulxin. *Blood*. 2006;107(8):3145–3152.
56. Broze GJ Jr, Yin ZF, Lasky N. A tail vein bleeding time model and delayed bleeding in hemophiliac mice. *Thromb Haemost*. 2001;85(4):747–748.
57. Zhang G, et al. Biphasic roles for soluble guanylyl cyclase (sGC) in platelet activation. *Blood*. 2011;118(13):3670–3679.
58. Chrzanowska-Wodnicka M, Smyth SS, Schoenwaelder SM, Fischer TH, White GC 2nd. Rap1b is required for normal platelet function and hemostasis in mice. *J Clin Invest*. 2005;115(3):680–687.